



*LIGO Laboratory / LIGO Scientific Collaboration*

LIGO-T050086-00-R

*ADVANCED LIGO*

6/20/2005

---

Proposal for a Homodyne (DC) Detection Experiment at  
the LIGO Caltech 40-Meter Laboratory

---

Ben Abbott, Rana Adhikari, Daniel Busby, Jay Heefner, Keita Kawabe, Osamu Miyakawa, Virginio Sannibale, Mike Smith, Monica Varvella, Steve Vass, Rob Ward, Alan Weinstein

Distribution of this document:  
LIGO Science Collaboration

This is an internal working note  
of the LIGO Project.

**California Institute of Technology**  
LIGO Project – MS 18-34  
1200 E. California Blvd.  
Pasadena, CA 91125  
Phone (626) 395-2129  
Fax (626) 304-9834  
E-mail: info@ligo.caltech.edu

**Massachusetts Institute of Technology**  
LIGO Project – NW17-161  
175 Albany St  
Cambridge, MA 02139  
Phone (617) 253-4824  
Fax (617) 253-7014  
E-mail: info@ligo.mit.edu

**LIGO Hanford Observatory**  
P.O. Box 1970  
Mail Stop S9-02  
Richland, WA 99352  
Phone 509-372-8106  
Fax 509-372-8137

**LIGO Livingston Observatory**  
P.O. Box 940  
Livingston, LA 70754  
Phone 225-686-3100  
Fax 225-686-7189

<http://www.ligo.caltech.edu/>

**Table of Contents**

**1 INTRODUCTION – DC READOUT AT THE 40M.....1-1**

1.1 HETERODYNE & HOMODYNE READOUTS..... 1-1

    1.1.1 *Anticipated advantages of DC readout:*..... 1-2

    1.1.2 *Potential disadvantages of DC readout:*..... 1-3

    1.1.3 *Homodyne phase angle:*..... 1-4

**2 DC READOUT AT THE 40 METER .....2-5**

2.1 WHAT CAN WE LEARN FROM DC READOUT AT THE 40M?..... 2-5

2.2 DC READOUT GW TRANSFER FUNCTIONS..... 2-6

2.3 CONTROLLING THE DC DARM OFFSET ..... 2-7

**3 ELEMENTS OF DC DETECTION BEAMLINE.....3-10**

3.1 IN-VACUUM STEERING MIRRORS..... 3-12

3.2 MODE MATCHING TELESCOPE (MMT)..... 3-12

3.3 OUTPUT MODE CLEANER (OMC)..... 3-13

    3.3.1 *Controlling the OMC* ..... 3-20

3.4 DC DETECTION PHOTODIODES..... 3-20

**4 CONSTRUCTION AND INSTALLATION SCHEDULE.....4-22**

**5 BUDGET .....5-22**

**6 OUTSTANDING QUESTIONS AND FURTHER PLANS .....6-24**

6.1 FURTHER PLANS..... 6-24

## 1 Introduction – DC readout at the 40m

Homodyne detection (via a DC readout scheme) has been chosen as the baseline readout scheme for AdLIGO. DC Readout eliminates several sources of technical noise, as discussed below. The LIGO Caltech 40 meter laboratory (the 40m) is currently prototyping a suspended, power-recycled, detuned RSE optical configuration for AdLIGO. A complete prototyping of the AdLIGO optical configuration, in our view, includes the readout method.

From its inception in 2000, our plan for the upgraded 40 meter interferometer has been to

- design and construct a dual-recycled Fabry-Perot Michelson (DRFPMI) interferometer as close as possible to the AdLIGO design;
- develop procedures to acquire lock and control the DRFPMI interferometer in preparation for the commissioning of AdLIGO;
- study the response of the interferometer, including RSE and optical spring effects;
- understand and minimize the noise;
- develop, implement and study the performance of DC readout schemes;
- operate the interferometer as a facility for testing additional LIGO innovations.

We are currently in advanced stages of learning how to acquire lock and control the DRFPMI interferometer, and the time is right (from the perspective of the 40m schedule) to develop, implement, and test a DC readout scheme. This document outlines our current thinking on the design of a first test.

### 1.1 Heterodyne & homodyne readouts

Heterodyne detection is the traditional RF modulation/demodulation scheme for extracting information on the state of resonance of the main laser beam in the optical cavities of the interferometer, which is used to control the mirror positions and the laser in order to maintain the desired resonant state. It involves:

- RF phase modulation of input beam (in the case of Initial LIGO and the 40m, this modulation is applied on the PSL table before the input mode cleaner).
- Optical cavity lengths chosen to transmit first-order RF sideband(s) to anti-symmetric (AS) output port with high efficiency (Schnupp asymmetry).
- For Initial LIGO, the RF sidebands are in principal balanced at the AS port
- For the AdLIGO design with detuned RSE, one RF sideband is much stronger than the other at the AS port; in fact, *any* RF sideband with a resonance condition that is not identical to that of the carrier will have some imbalance.
- RF sideband(s) serve as local oscillator (RFLO) to beat with GW-produced field from differential motion of the arms.
- The linear GW signal is extracted from the amplitude modulation of RF-demodulated photocurrent.

Homodyne detection (of the GW wave signal) via DC readout makes no use of RF sidebands. In this scheme:

- A controlled amount of carrier light is made to exit the AS port by introducing a differential offset in the arm lengths (DARM) or the Michelson (MICH dark fringe) degrees of freedom, via the control system
- The main laser field (carrier) serves as local oscillator (DCLO) at the AS port to beat with GW-produced field from differential motion of the arms at GW (audio) frequencies
- The linear GW signal is extracted from the amplitude modulation of the GW-band photocurrent

Introducing a controlled amount of DC laser light out the otherwise-dark AS port effectively allows the GW-modulated light to be detected with a linear response, as illustrated in Figure 1.

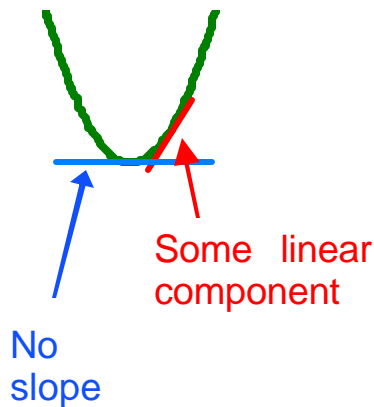


Figure 1. DC offset at AS port allows a linear GW-modulated signal to be extracted

### 1.1.1 Anticipated advantages of DC readout:

DC Readout eliminates several sources of technical noise (mainly due to the RF sidebands):

- RF local oscillator (RFLO) phase noise.
- Poor, unstable, or mode-mismatched RF field buildup in the marginally-stable and thermally-loaded power recycling cavity.
- Poor spatial overlap of the RFLO and GW signal at the AS port PD.

With DC readout,

- The carrier light will serve as a heavily stabilized local oscillator (DCLO), filtered by the double-pole of the power-recycled Fabry-Perot coupled cavities.
- There will be a perfect spatial overlap of the DCLO and GW signal at PD.

In the context of AdLIGO:

- In the detuned RSE configuration, the RF sidebands at the AS port are unbalanced; essentially, one sideband exits at the AS port and the other is almost completely reflected to the SP port. This will introduce *new* noise couplings for RF detection. DC detection avoids these problems.
- AdLIGO will utilize an output mode cleaner (OMC) to reject junk light (not containing GW signal information; due to Michelson contrast defect, mode mismatching, etc) at the AS port. This OMC can also reject the noisy RF sidebands, leaving only arm-filtered carrier and GW signal sidebands. An OMC which passes the RF sidebands is more complex.

- A pickoff before the OMC will permit standard RF detection as well, to aid in lock acquisition and to provide a backup for DARM control and GW signal extraction.
- Homodyne detection can yield slightly improved quantum noise (see Figure 2).
- DC Readout has the potential for QND measurements, without major modifications to the IFO.

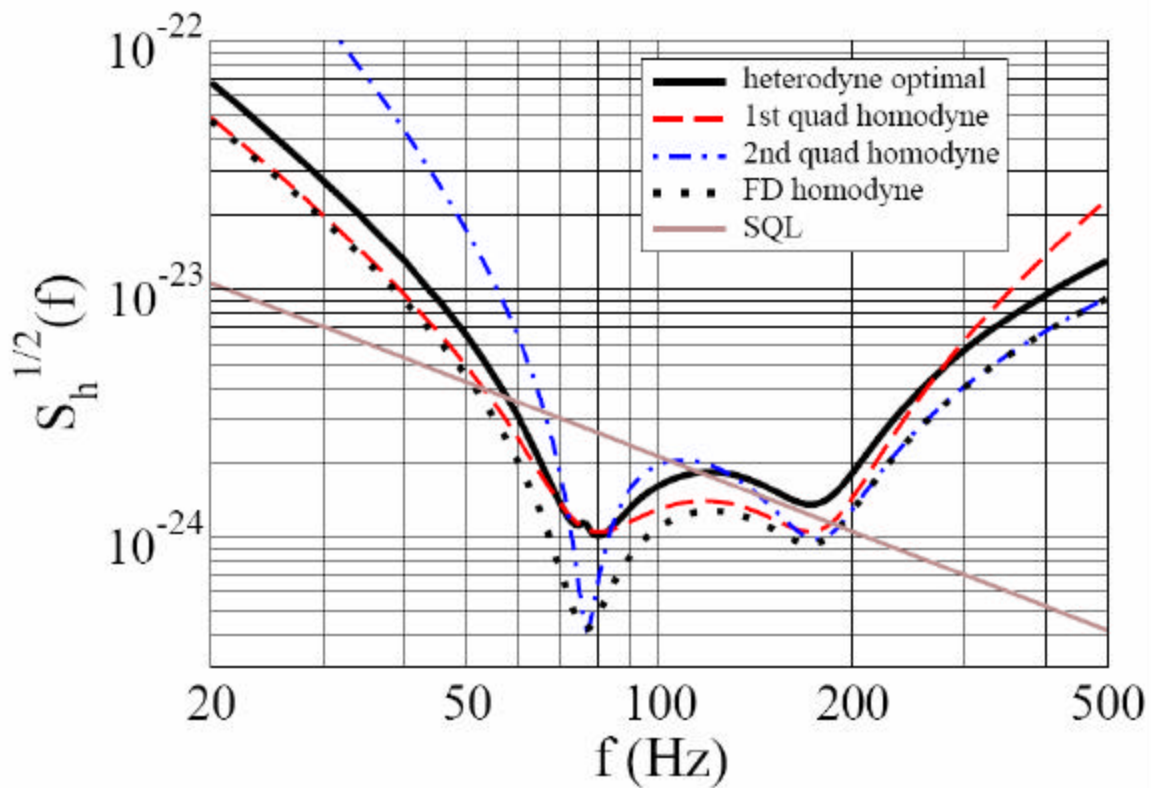


Figure 2: A comparison of predicted quantum noise using heterodyne (RF) and homodyne (DC) detection (Buonanno, Chen, Mavalvala, Phys.Rev. D67 (2003) 122005). For heterodyne sensing, a single optimal demod phase is chosen; for homodyne detection, two possible demod phase angles are studied. The SNR for NS-NS binaries is  $\sim 5\%$  higher for homodyne detection than for heterodyne (with spherical mirrors).

### 1.1.2 Potential disadvantages of DC readout

- Much higher environmental noise at low frequency. DC detection requires seismic and acoustic isolation of the OMC and DC photodetector.
- Photodetector and electronic noise ( $\sim 1/f$ ) at low frequency. The only additional source of  $1/f$  noise is the photodetector itself. Otherwise, our exposure to this type of noise is identical to the RF detection case.
- Intensity stability – laser intensity fluctuations couple directly to the GW signal.
- There are two components of the local oscillator, in DC readout:

- Field from intentional offsets, in order to deliver the filtered local oscillator out the AS port
- Field arising from imbalanced arms (differences in arm reflectivities) or contrast defect of the Michelson. The effect of different transverse profiles from the arms is minimized by the presence of the OMC; it becomes a source of loss rather than a source of noise.
- These two components of the local oscillator appear in different quadratures, making it possible to choose and control the homodyne phase angle. However, the first component is under our control while the second is not, and is likely to be time-varying in an uncontrollable and difficult-to-monitor way. Such fluctuations can mimic the GW signal and thereby be a new source of noise.

### 1.1.3 Homodyne phase angle

- There are two components of local oscillator, in DC readout:
  - Carrier field due to intentional dark fringe offset (of DARM or MICH), in order to deliver the filtered local oscillator out the AS port
  - Carrier field arising from unbalanced arm reflectivity (due to ITM reflectivity mismatch, arm loss mismatch, or contrast defect of the Michelson).
  - There is also a carrier field from mismatch of the transverse profile due to higher order modes in the recycling cavity, but the output mode cleaner should reject these.

The dark fringe offset is under our control while the carrier field arising from unbalanced arm reflectivity is not. This means that it is difficult to choose and control the homodyne detection phase angle  $\beta$ . See Figure 3.

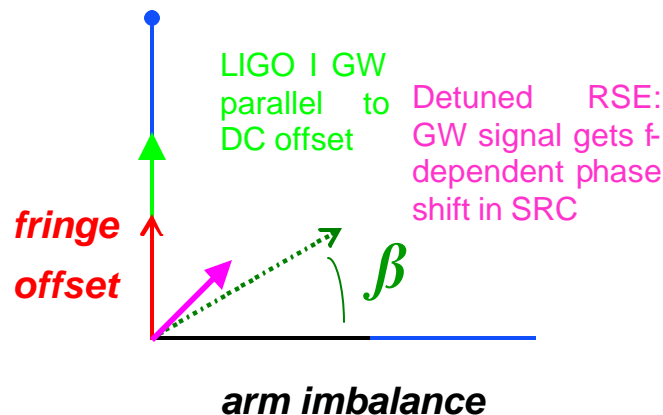


Figure 3: Homodyne phase angle  $\beta$ , formed from the vector sum of the intentional dark fringe offset (which has the same phase as the GW) and the uncontrollable arm imbalance.

The homodyne detection phase angle  $\beta$  should be parallel to the GW signal phase; however, due to the detuned RSE cavity, the phase angle of the GW signal is frequency dependent. We can estimate and measure the output power due to the existing arm imbalance at the 40m, and we can dial in any chosen dark fringe offset. the output power due to the arm reflectivity imbalance. In this way, we can explore and

optimize the homodyne detection phase angle  $\beta$ , in order to maximize the response to GW signals for some frequencies, but not all. Initial studies indicate that for reasonable assumptions about the arm imbalance, offsetting DARM by anywhere from 0-20 pm will allow us to choose any homodyne angle from 0-90 degrees. We also need to consider the rms offset in DARM due the finite gain of the DARM servo. Hopefully we can get this number fairly well below 1 pm, making intentional offsets as small as 3 pm meaningful.

## 2 DC readout at the 40 meter

As mentioned above, Homodyne detection (via a DC readout scheme) has been chosen as the readout scheme for AdLIGO, because of its potential for eliminating several sources of technical noise (mainly due to the RF sidebands). The 40m is currently prototyping a suspended, power-recycled, detuned RSE optical configuration for AdLIGO. A complete prototyping of the AdLIGO optical configuration, in our view, includes the readout method.

### 2.1 What can we learn from DC Readout at the 40m?

At the time of writing (May 2005), the 40 meter interferometer has not yet been brought into its intended optical configuration (DRFPMI). For reference, the last time we measured a calibrated noise spectrum (in the un-recycled Fabry-Perot Michelson configuration) was in December, 2003; see Figure 4. It is clear that there is a long way to go. It should also be remembered that the typical seismic noise at Caltech is roughly an order of magnitude worse than at LHO, our seismic stacks (especially for the mode cleaner) do not perform as well as the ones at the sites, and our test masses are only 1.4 kg. Due to these effects, we expect to have considerably larger displacement noise than the sites, below 100 Hz.

We expect to lock the full DRFPMI in the next few months, establish a reliable lock acquisition procedure for AdLIGO, measure the response to large-amplitude GWs (via swept-sine excitations) and compare with expectations. When we do achieve this milestone, we will begin the job of identifying and eliminating the many sources of technical noise that typically plague complex interferometers. We do not expect to be able to operate with a noise spectrum that is limited by fundamental noise sources, for some time. Our current goals for the 40m DRFPMI prototype with RF detection include only an initial look at noise sources, not an exhaustive battle with them.

This will be a good time, and place, to test homodyne detection. Our initial goal is to implement a DC detection optical beamline, sensing and control electronics. This can be done on an existing seismic stack in (small) vacuum chamber, already in place for this purpose.

It is not clear how much can be learned about limits to noise in homodyne detection, in the 40 meter environment. Given the expected noise, we're not likely to see any quantum effects associated with homodyne detection, for some time. We may not even see any noise improvements. Our primary goal, at this stage, is simply to learn how to implement the system:

- How to build, lock and control the output mode cleaner?
- How best to control the DARM offset?
- Can we measure the expected response to large-amplitude GWs, using swept-sine excitations?
- What are the unforeseen noise sources associated with an in-vacuum OMC?
- How do we make a good in-vacuum photodiode? What unforeseen noise sources are associated with it?
- We hope to discover any other unforeseen pitfalls.

- We will also perform as thorough an investigation as we can regarding noise couplings in detuned RSE, with both heterodyne and homodyne detection. This will involve parallel efforts in both modeling and measurement.

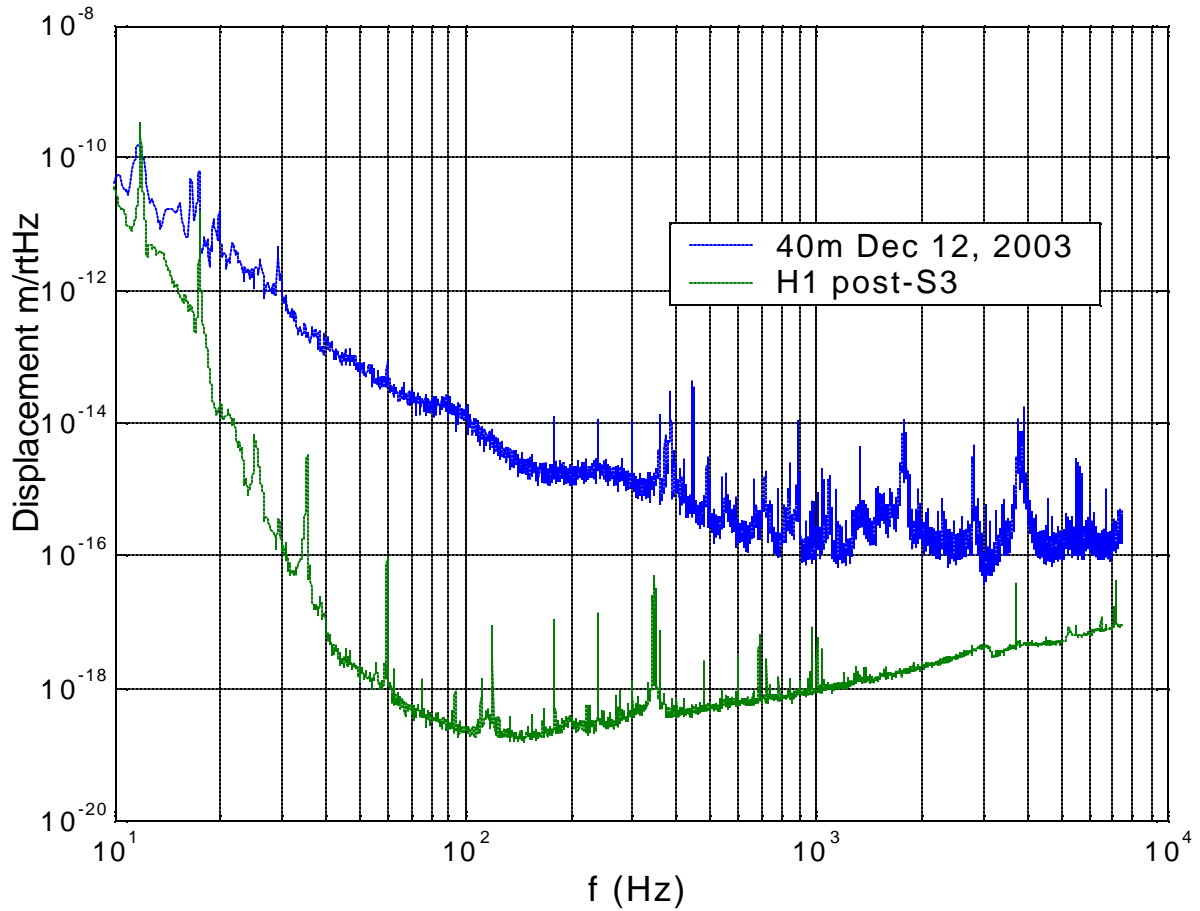


Figure 4: Calibrated displacement noise spectrum from the 40 meter interferometer in the un-recycled Fabry-Perot Michelson configuration in December, 2003 (blue), compared with H1 post-S3.

## 2.2 DC Readout GW Transfer Functions

The DC detection response of the 40 meter DRFPMI to a GW signal in DARM is shown in Figure 5, based on calculations done with a FINESSE model. The signal cavity at the 40 meter is detuned to be resonant at 4 kHz, hence the peaks there. In the absence of intentional DC offset, the signal derives from carrier light LO from the small arm reflectivity unbalance. Intentionally adding a DC offset (in pm) to the DARM degree of freedom changes both the amplitude and phase of the local oscillator.

A DC offset can be applied via the Length Sensing and Control (LSC) system, and it can be automated. It would be applied only after acquiring lock and achieving stable control of the interferometer. A calibration procedure would be required in order to apply an offset that corresponds to a known displacement, making use of monitors of the power level in the arms.

The amount of DC offset requires optimization. We want a DC offset that is large enough to provide a robust signal at the DC readout photodiode, and relatively insensitive to the (anticipated) amount of uncontrolled local oscillator due to arm imbalance (which affects the homodyne detection phase angle  $\beta$ ). If the DC offset is too large, the light stored in the arms will begin to decline. Referring to Figure 5, we'll plan on a  $\sim 19$  pm offset. For AdLIGO, with much higher laser power, a much smaller offset would be desirable.

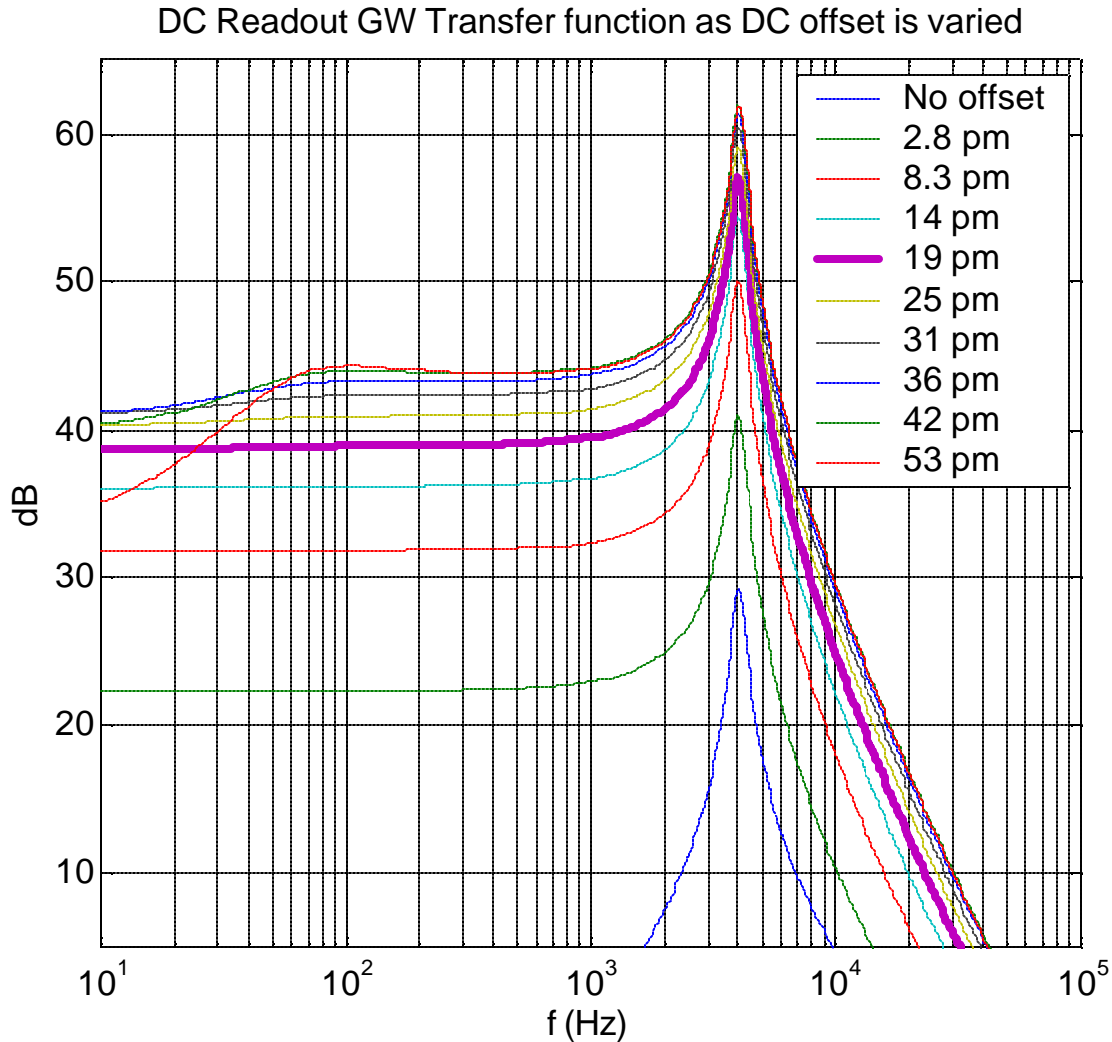


Figure 5: Transfer function from GW (DARM) signal to DC readout at the 40 meter dual-recycled Fabry-Perot Michelson interferometer, as a function of GW frequency, for different DC DARM offsets. The signal cavity at the 40 meter is detuned to be resonant at 4 kHz, hence the peaks there. In the absence of intentional DC offset, the signal derives from carrier light LO from the small arm reflectivity unbalance, taken to be XX. Modeling done with FINESSE.

### 2.3 Controlling the DC DARM offset

The DARM offset needed to produce the DCLO can be produced by offset-locking the arms or the Michelson. In both cases, the resulting DCLO exiting the AS port will benefit from filtering of the carrier light by the coupled-cavity pole (PRC & arms). The expression below (from seminal paper by Camp/Yamamoto/Whitcomb/McClelland, J. Opt. Soc Am 17, 120) shows that the carrier field exiting the AS port receives contributions from an arm offset ( $dx_a$ ) amplified by the arm gain ( $G_a$ ), as well as from a Michelson offset from the dark fringe ( $dx_r$ ). Both contributions are filtered by the coupled-cavity pole  $\omega_c$ .

$$E_d^c = \frac{E_m^c}{2} t_r G_r^c \times \left[ \frac{A_{cm} \left( 1 + i r_f \frac{\omega}{\omega_c} \right) + i G_a k dx_{a-} + i k dx_{r-}}{\left( 1 + \frac{i \omega}{\omega_{cc}} \right)} \right], \quad (23)$$

For the 40 meter, the coupled-cavity pole frequency  $\omega_c / (2\pi)$  is around 60 Hz; for AdLIGO it is around 0.6 Hz.

The offsets can be applied as digital offsets to the DARM or MICH controls in the LSC system, which are derived from signals from the LSC RFPDs. As far as introducing any required carrier DC offset at the AS port is concerned, both these approaches work equivalently. However, some initial modeling with T. Corbitt's code and with FINESSE show that the frequency noise is worse at high frequencies with a MICH offset than a DARM offset. This seems to be due to the fact that laser noise sidebands above the arm cavity poles fall out of resonance in the arms, and so don't see the coupled cavity pole. If the Michelson is offset, these sidebands experience much less common mode rejection.

Operationally the two types of offsets require different servo implementations. They can also affect the GW signal sidebands differently: applying an offset to MICH will not introduce any additional GW signal sideband phase shift (as a function of frequency), whereas applying an offset to DARM will affect the double cavity GW signal sideband frequency dependence; the RSE peak will shift in frequency. This is probably a negligible effect, and, of course, the SRC length can be re adjusted in this case to give identical response to the DARM offset. It is likely that for the parameters of interest in AdLIGO the GW signal response "distortion" inherent in the DARM offset method is negligible.

Note that our step-by-step lock acquisition procedure also makes use of DC locking of the arms to the transmitted light power signal as an intermediate step. The offset can be applied there, as well. Figure 6 shows the expected DARM signals that can be obtained by applying a DC offset using RF or DC signals. Notice that the difference between the ARM transmitted powers (TRX-TRY) gives a DARM signal; this is an effect of the detuned signal cavity. The square root of the AS port power also gives a nice DARM signal in a certain region. A 19 picometer offset is well into the linear regime of the AP power signal. The LO power is about 9mW (for 1W after the MC). Note that the TRX-TRY signal has an offset due to the arm imbalance.

When an offset is applied to DARM, an offset is also generated in the CARM signal derived from demodulation of the light at the SP port at 33 MHz, as illustrated in Figure 7, unless the demod phase is tuned with exquisite precision. This may have some effect on the Common-Mode servo. Also, it means that the power at the BS is reduced by a small amount (~3% in this simulation).

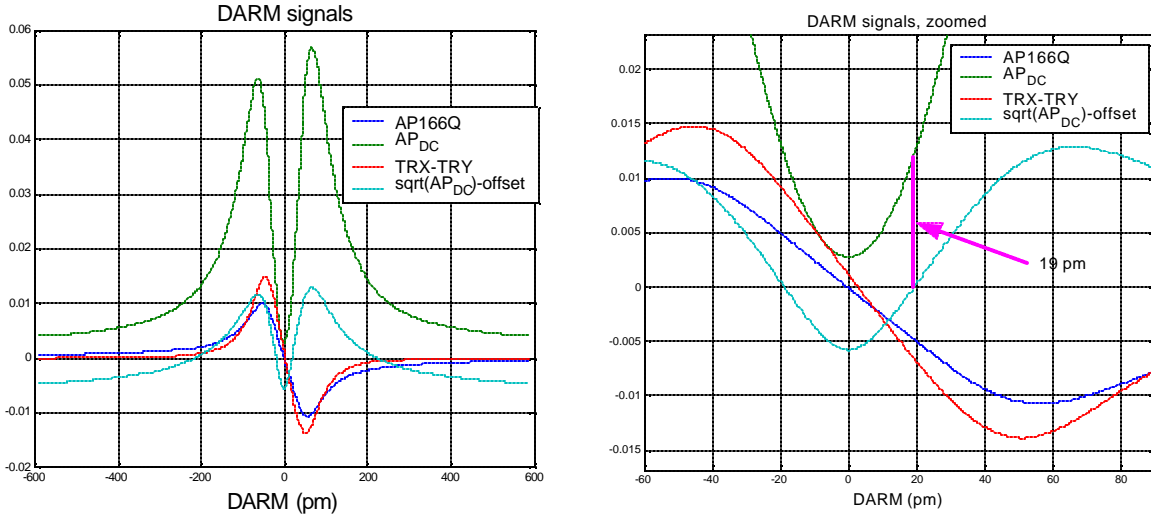


Figure 6: Various ways of obtaining the DARM signal at the 40m DRFPML. The standard RF approach, using the 166 MHz signal at the AS port, is shown in dark blue. The other signals are derived from DC power at the AS port or at the TRX and TRY arm transmitted ports. The right plot is a close-up of the left one, in the vicinity of the operating point. The proposed DC offset is shown; its slope is sensitive to DARM and relatively insensitive to the presence of uncontrolled DCLO light due to the expected arm imbalance.

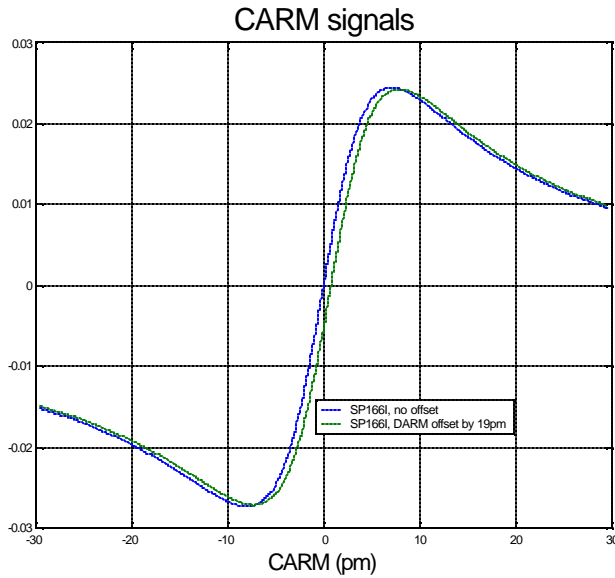


Figure 7: The CARM signal derived from demodulation of the light at the SP port at 33 MHz.

### 3 Elements of DC detection beamline

Currently, light exiting the AS port through the signal mirror goes straight out of the vacuum chamber and into an RF detection beamline (AP1) on a nearby optical table. This includes a mechanical shutter, a high-frequency (166 MHz) LSC RFPD, a double-demod (DD) LSC RFPD, a QPD, CCD camera, and optical spectrum analyzer; see Figure 8.

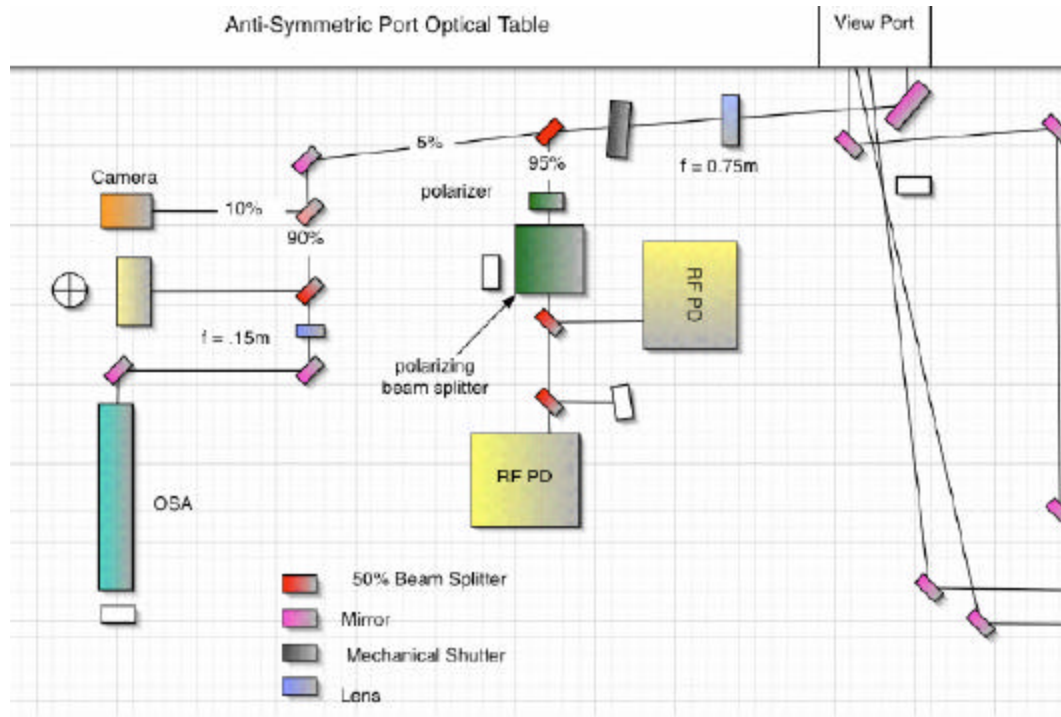


Figure 8: The current AP1 beamline at the AS port.

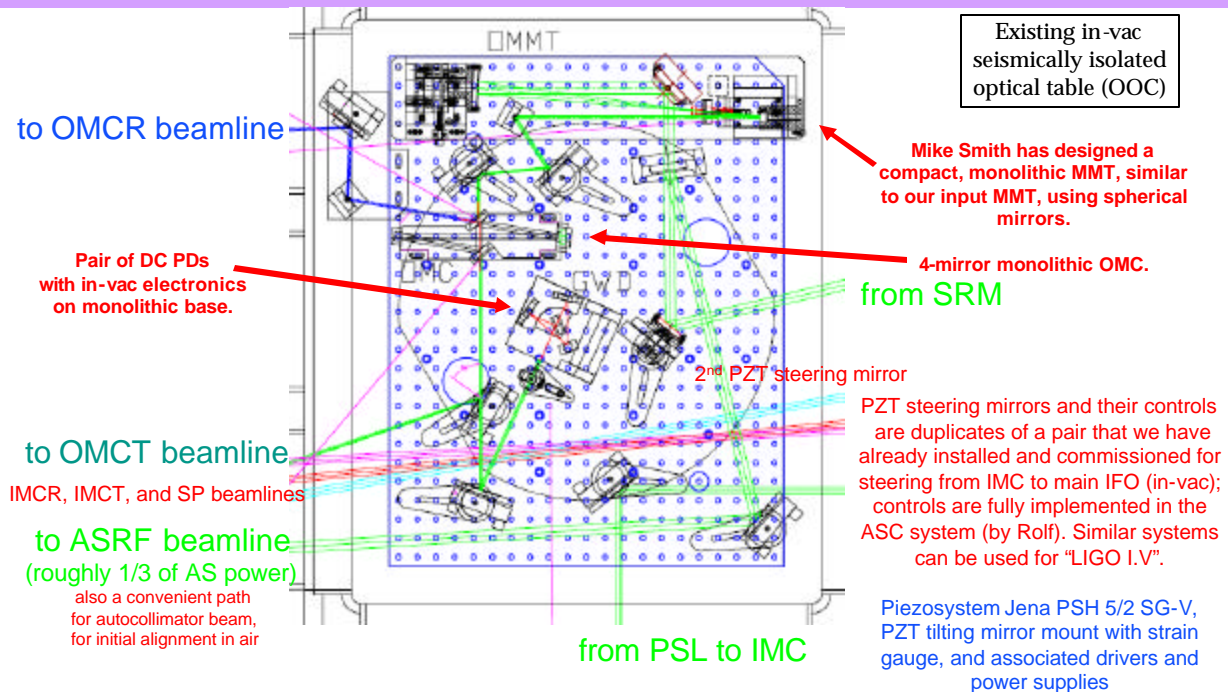
The current plan is to pick off some (most) of the light exiting the AS port, before it exits the vacuum envelope, and send it into DC detection system. The system would be composed of elements in the vacuum chamber, on existing seismic stacks (thus, seismically- and acoustically isolated). The elements of the beamline (AP2) would include:

- Two in-vacuum steering mirrors (PZT, potentially servo-controlled);
- A mode matching telescope (rather short, monolithic, fixed mirrors with remote control focus);
- Output mode cleaner (3- or 4-mirror, fixed spacer, PZT-mounted mirror);
- In-vacuum DC detection bare photodiode with in-vacuum wiring to...
- an in-air preamplifier placed very close to the vacuum electrical feed through;
- An OMC reflected beamline (on optical table in air);
- An OMC transmitted beamline (on optical table in air);





# Output Optic Chamber



LIGO-G050324-00-R

DC Detection at the 40m Lab

Mike Smith

11

Figure 10: Preliminary layout of the in-vacuum detection beamline in the Output Optic Chamber (OOC).

## 3.1 In-vacuum steering mirrors

The beam exiting the AS port through the signal mirror will encounter one in-vacuum PZT steering mirror on the BS chamber table, followed by a second PZT steering mirror on the Output Optic Chamber (OOC). This will allow us to correct for drifts between the two tables, and to steer the beam precisely onto the MMT and OMC after pump-down. An external camera will view the beam incident on the MMT through a vacuum view port. It may be possible to implement a servo to continuously steer the beam.

These in-vacuum PZT mirrors can be identical to the pair that is currently installed and in use to steer the beam from the input mode cleaner to the main interferometer (Piezo-Jena mirror tilting actuator with positioning feedback sensor and controller).

## 3.2 Mode matching telescope (MMT)

Mike Smith has designed a rather short, monolithic, device with fixed mirrors with remote control piezomotor focus adjustment, very similar to the one already built, installed and in use to mode match the beam from the input mode cleaner to the main interferometer. The IMC→IFO MMT makes use of off-axis parabolic mirrors to minimize astigmatism introduced by the short MMT. For the proposed IFO→OMC

MMT, we can tolerate some astigmatism. Mike has chosen off-the-shelf spherical mirrors which effectively mode-match the beam to the OMC while introducing only a very small astigmatism (X%).

### 3.3 Output mode cleaner (OMC)

An OMC at the AS port is required to pass the TEM<sub>00</sub> mode carrier light from the arms, rejecting any higher order modes (HOMs) from the PRC, and all the RF sidebands. The output MMT will mode-match the TEM<sub>00</sub> mode into the OMC. Design considerations:

- Environmental noise will introduce amplitude fluctuations in the transmitted light, which will appear as GW signal at the DC photodiode. The OMC should be seismically and acoustically isolated. Therefore, we will locate the OMC on a seismic stack in the vacuum envelope (in the Output Optic Chamber OOC which was installed at the vertex of the 40m IFO for precisely this purpose).
- Space on the OOC optical table is limited, so we need to make the OMC rather short.
- To keep it simple, we propose to build a small OMC with a fixed spacer, as a monolithic block, with off-the-shelf mirrors. The spacer can be made out of aluminum or invar. If we build something quick and cheap, we can learn a lot before building a more elaborate device (if necessary).
- In order to reject RF sidebands and HOMs, we need to ensure that they don't accidentally resonate on a FSR line; so, we want a reasonably high finesse (say, ~100-500); but not too high, or it will be difficult to lock and control.
- We will choose an off-the-shelf spherical mirror which will produce a Gouy phase shift for HOMs that will minimize their transmission.
- A three-mirror design can be very similar (or even identical to) a PSL pre-mode-cleaner (PMC), consisting of a flat input coupler, a flat output coupler, and a PZT-actuated curved mirror.
- With a three-mirror design, TEM<sub>mn</sub> modes with  $m$  odd and  $n$  even will resonate with a different phase than those with  $m$  even and  $n$  odd, whereas those two modes are degenerate in cavities with 4 (or an even number) of mirrors. Thus, a 3-mirror cavity produces twice as much chance of accidental HOM resonances. For this reason, it may be better to use a 4-mirror design. See Figure 11.
- However, it may be that the problem of accidental HOM resonances is sufficiently small that a (simpler?) 3-mirror design is adequate. We plan to measure the transverse profile of the AS port beam to see how important these HOMs are.
- Because the OMC will be rather short, the incident angle on the curved mirror will be relatively steep, leading to astigmatism of the output beam. We would like to choose an OMC geometry (aspect ratio) that minimizes this. However, the beam will be immediately directed towards a DC photodiode, so the presence of astigmatism is not really a problem, other than the loss due to the coupling inefficiency.
- The beam should be incident on all mirrors at a rather steep angle with respect to normal incidence, in order to avoid back-scattered light from the input coupler returning to the IFO, or counter-propagating light in the OMC cavity. This requirement is in direct opposition to the requirement for a small astigmatism.

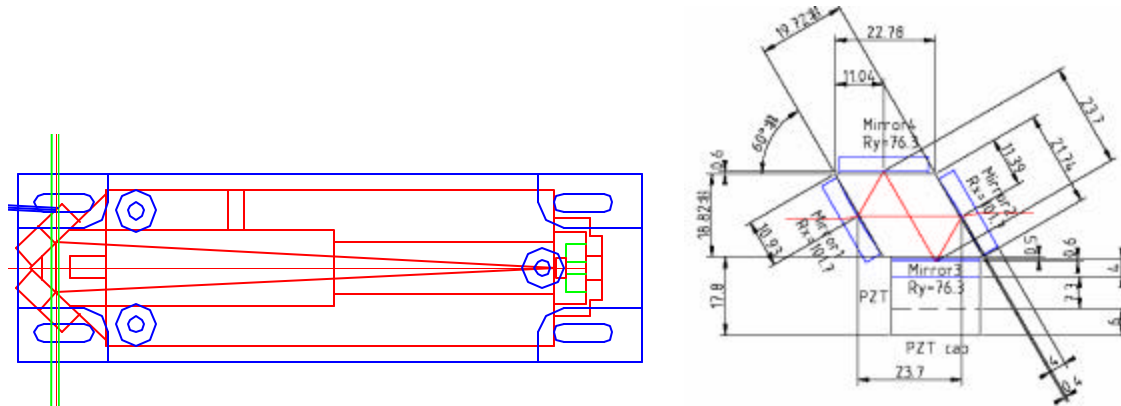


Figure 11: Left: The 3-mirror PMC design, with PZT-actuated curved mirror on the right (cavity half-length = 21 cm). Right: Design by Keita for 4-mirror cavity, with flat input coupler on the left, flat output coupler on the right, flat PZT-actuated mirror on bottom, and spherical mirror on top.

Parameters for a strawman design, based on the PSL pre-mode-cleaner, are shown in Figure 12.

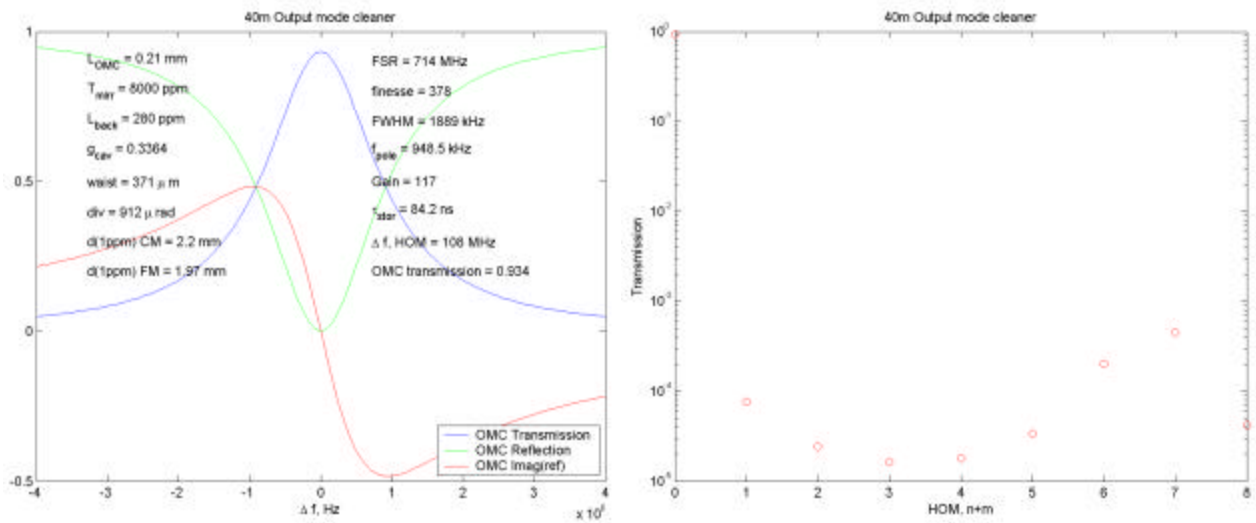


Figure 12: Left: Parameters for an OMC based on the PSL PMC. Right: Transmission of higher order modes, versus  $n+m$ .

### 3.3.1 OMC Length

The primary purpose of the OMC is to reject (reflect, or filter out) the HOMs of the carrier light, the RF sidebands at  $\pm 33.207 \text{ MHz}$  and  $\pm 166.03 \text{ MHz}$ , and HOMs of the RF sidebands. The lowest-order  $\text{TEM}_{00}$  mode is defined by the arm cavities. As the beam propagates through the SRM and the output mode-matching telescope (OMMT), the  $\text{TEM}_{00}$  mode of the arms is made to be nearly identical to the  $\text{TEM}_{00}$  mode of the OMC. We will therefore consider the transmission of OMC modes, although it should be kept in mind that these are not identical to the arm modes.

The transmission of the various frequency and mode components of the beam is governed by the OMC finesse (which we will here take to be 300, resulting in a carrier TEM<sub>00</sub> mode transmission of 96% ), the radius of curvature of the concave curved mirror (which we will here take to be 1 meter so that we can use spare PMC mirrors), and the cavity length. The presence of the concave curved mirror means that the OMC resonant modes will be well-separated in Guoy phase, so that if the carrier TEM<sub>00</sub> mode is made to resonate in the OMC, the HOMs will not, so long as a suitable choice of the cavity half-length  $L_{1/2}$  is made. We wish to specify a cavity half-length  $L_{1/2}$  which minimizes the transmission of the carrier and RF HOMs (as well as the lowest-order mode of the RF sidebands), and which is tolerant of small errors in  $L_{1/2}$  and in the radius of curvature of the curved mirror.

The power transmission of the TEM<sub>m</sub> mode of the carrier or RF sideband is given by:

$$T_{OMC} = \left| \frac{t_1 t_2 e^{i\mathbf{f}_1}}{1 - r_1 r_2 r_3 r_4 e^{i\Delta\mathbf{f}_r}} \right|^2$$

where  $\mathbf{f}_1$  is the phase advance of the beam while propagating from the input coupling mirror to the output coupler,  $t_1$  and  $t_2$  are the amplitude transmissions of the input and output coupling mirrors, the  $r$ 's are the amplitude reflectivities of the four mirrors, and

$$\Delta\mathbf{f}_r = \Delta\mathbf{V} + 2\mathbf{p} \cdot 2L_{1/2}f_{rf} / c$$

$$\Delta\mathbf{V} = 2 \tan^{-1} \left( \frac{1}{\sqrt{R/L_{1/2} - 1}} \right) = 2 \cos^{-1} \sqrt{1 - L_{1/2} / R}$$

where  $L_{1/2}$  is the cavity half-length,  $f_{rf}$  is the RF frequency (0 for the carrier, or  $\pm 33.207$  MHz or  $\pm 166.03$  MHz for the sidebands),  $R$  is the radius of curvature of the curved mirror, and  $\Delta\mathbf{V}$  is the round-trip Guoy phase for the modes with  $n+m=1$ .

We take  $|t_1|^2 = |t_2|^2 = T_1 = T_2 = 1\%$ , and all four mirrors have losses of 100 ppm. This yields a finesse of 306, a pole frequency of  $\sim 1$  MHz (and FWHM of  $\sim 2$  MHz), and carrier TEM<sub>00</sub> mode transmission of 96%.

Below, we plot the transmission versus cavity half-length  $L_{1/2}$  for various cases. We focus on values of  $L_{1/2}$  near 0.25 m, since that is consistent with the available table-space in the 40 meter Output Optic Chamber (and is similar to the PSL PMC).

If we choose a cavity half-length  $L_{1/2}$  between 0.23 and 0.25 m, modes with  $m+n$  between 0 and 5 will be rejected at the  $10^{-3}$  level (Figure 14). Modes with  $m+n$  between 6 and 11 will be transmitted at greater than the  $10^{-2}$  level unless  $L_{1/2}$  lies between 0.234 and 0.242 m (Figure 13). Once we go beyond  $m+n=11$ , it gets increasingly difficult to avoid HOM resonances for any cavity length. Furthermore, if we make use of a cavity with only 3 mirrors, so that HOMs with odd  $m$  acquire an additional phase shift of  $\pi$ , it is difficult to avoid HOM resonances for  $m+n = 5$  (Figure 16 and Figure 17).

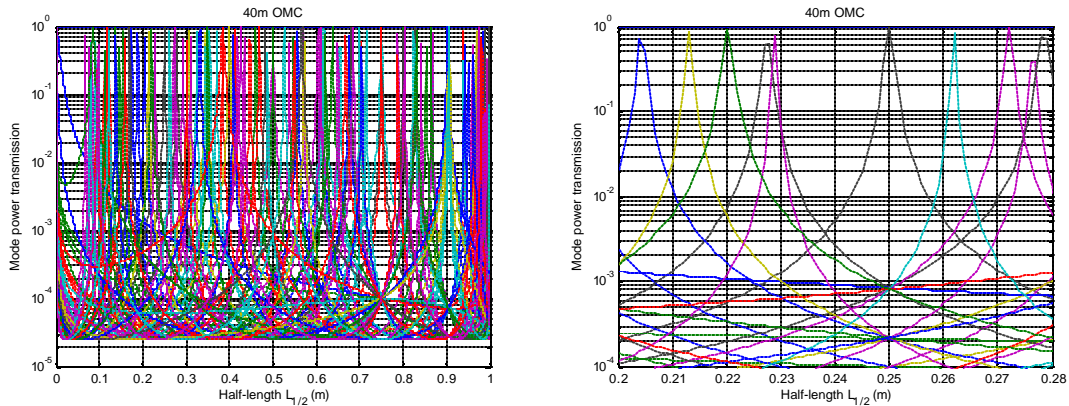


Figure 13: Transmission of carrier  $TEM_{00}$  (blue line at top at 0.96) and HOMs with  $m+n = 11$ , and RF sideband lowest-order and HO modes, versus cavity half-length, with one curved mirror with  $ROC = 1$  m. Left: Half-lengths from 0 to 1 m (corresponding to  $g$  factor ranging from 1 to 0). Right: zooming in on half-length around 0.24 m.

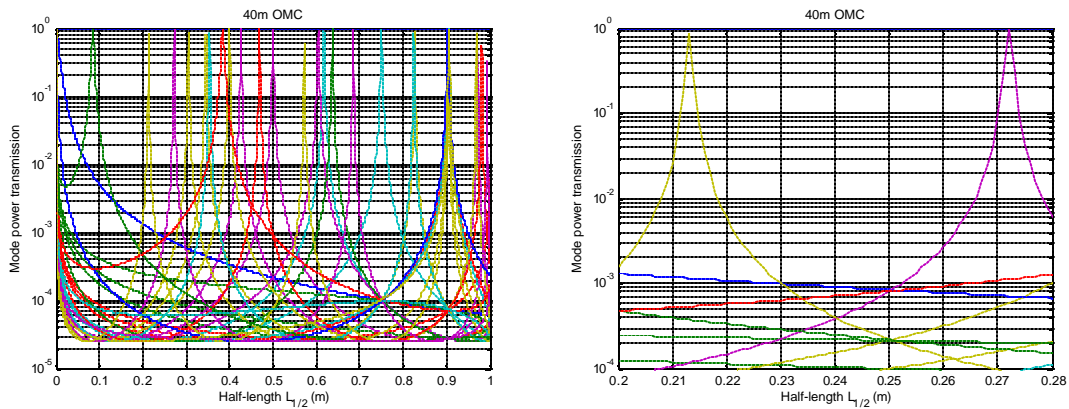


Figure 14: Same as Figure 13, except only HOMs with  $m+n = 5$ . The modes with  $m+n = 6$  begin to fill in the region between 0.22 and 0.27 m.

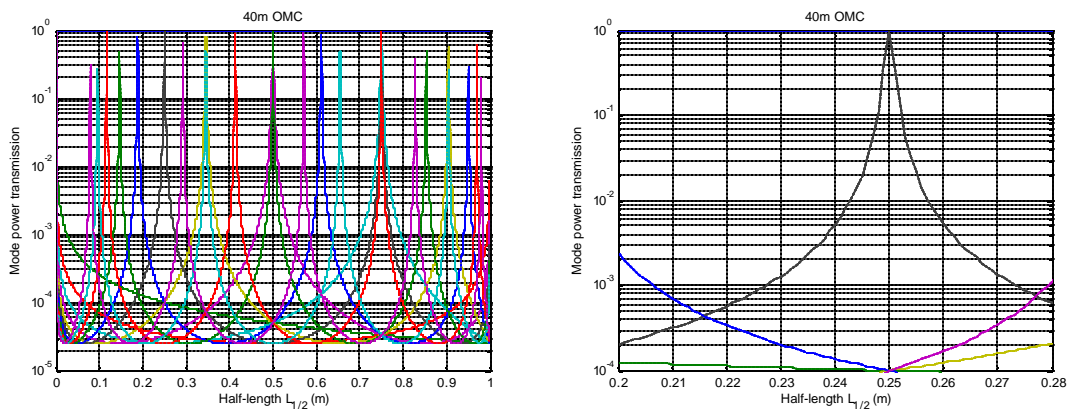


Figure 15: Same as Figure 13, except RF sidebands and their HOMs are excluded. Carrier modes up to  $m+n = 11$  are included.

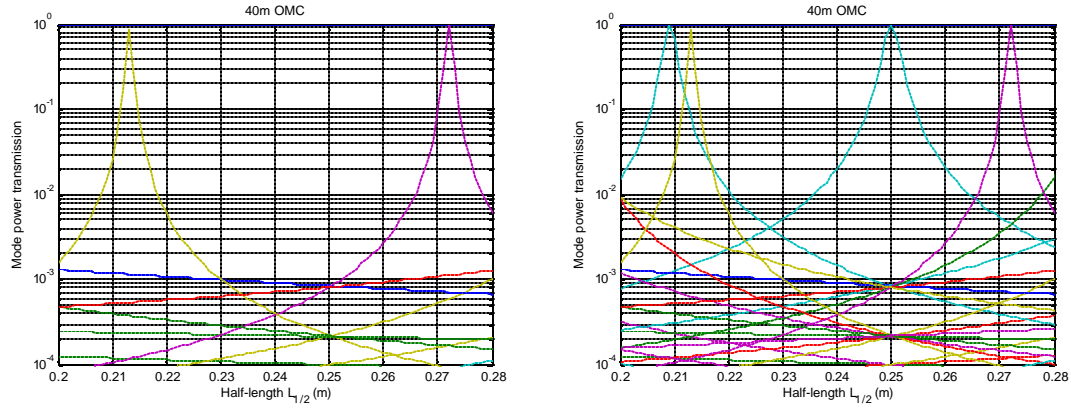


Figure 16: Transmission versus cavity half-length, for carrier and RF sidebands, modes with  $m+n = 5$  (as in Figure 14). Left: For a 4-mirror cavity. Right: For a 3-mirror cavity, where modes with odd  $m$  are shifted in phase by  $\pi$ .

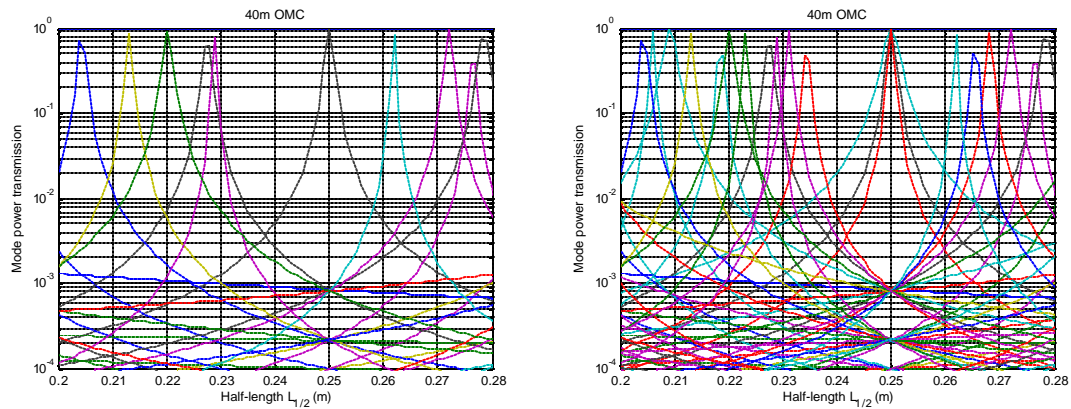


Figure 17: Same as in Figure 16, except all modes with with  $m+n = 11$  are included (as in Figure 13).

Based on these considerations, we choose a 4-mirror cavity, with curved mirror radius of curvature equal to 1 meter and  $L_{1/2}$  equal to 0.238 m. We can tolerate errors of up to  $\sim 3$  mm in the half-length and  $\sim 3\%$  in the radius of curvature.

### 3.3.2 OMC mechanical design

Mike Smith has designed a monolithic OMC in SolidWorks; see Figure 18. Materials: Aluminum, brass, or stainless steel, depending on thermal coefficient of expansion, stiffness (internal resonances), ease of machining, and cost. PZT. Mirror fixtures. Mirrors.

Material	Aluminum	Brass	Stainless Steel	Fused Silica	Invar
thermal expansion ( $10^{-6} / \text{K}$ )	25	20	11	0.55	0.6 – 1.3
Sound speed ( $10^3 \text{ m/s}$ )	6.4	3.7	5.8	6.0	

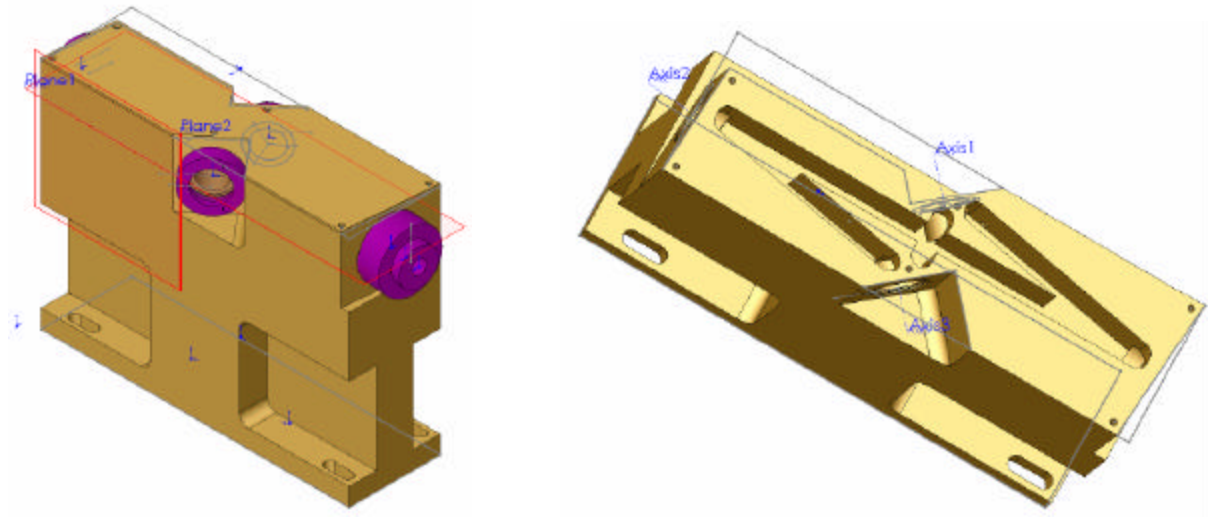


Figure 18: SolidWorks model of a monolithic OMC. Left: Overall view. Right: lifting the lid, here's the optical path for the 4-mirror design.

### 3.3.3 OMC mirrors

Assuming a 4-mirror cavity, the power transmission and finesse of the OMC cavity are shown in Figure 19.

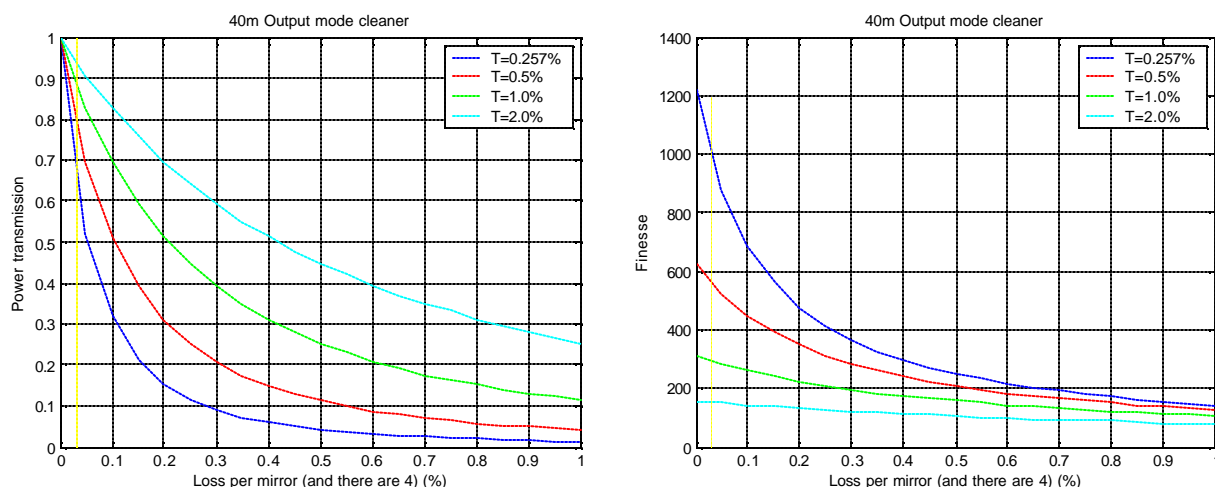


Figure 19: Left: Power transmission of the carrier TEM<sub>00</sub> mode-matched beam through the OMC, for different (matched) input/output coupler transmission, as a function of the loss per mirror in percent (assuming each of the 4 mirrors has the same loss; so multiply by 4 to get the total loss per round trip). Right: Finesse, for the same conditions.

The use of relatively poor-quality CVI optics could result in round-trip losses of a few percent, and thus in power transmission of 20% or less. This would be undesirable. Newport makes “super-polished” high-reflectance flats, but declined to quote on super-polished input/output couplers.

From the report of the Review panel for the 40m DC readout experiment (T050168):

It would be prudent to select output optics for low-scatter, although the cost and delivery schedule for low-scatter optics may be require the initial use of lower quality mirrors.

If we go with super-polished, specially-coated REO mirrors, the specs are summarized below. The cost would be ~ \$6700, and delivery would be 6 weeks ARO.

Mirror	Diameter	Thickness	Side 1	Side 2	wedge	Radius of curvature
M1	7.75 mm	4 mm	R > 99.9%, 0° inc	R < 0.2%	< 30 amin	1 m, CC/PL
M2	1”	0.25”	R ≥ 99.97%, 0° inc	R < 0.2%	< 30 amin	Flat PL/PL
M3	1”	0.25”	T ~ 1% , 45° inc, P-pol	R < 0.2%	30 amin	Flat PL/PL
M4	1”	0.25”	T ~ 1% , 45° inc, P-pol	R < 0.2%	30 amin	Flat PL/PL

Table 1: Mirror specs.

All mirrors are to be super-polished fused silica. Mirrors M3 and M4 are to be matched in transmission as closely as possible. The main beam is P-polarized (parallel to table, piercing the steering mirrors) everywhere from the Faraday Isolator, through the main IFO, and out to the sensing beamlines (it is S-polarized in the input mode cleaner).

### 3.3.4 Controlling the OMC

The OMC needs to be locked to the TEM00 carrier light. A length signal can be derived from dithering, PDH reflection, or tilt-locking. The suitably filtered signal can be fed back to the PZT-mounted mirror to acquire and maintain lock.

Dither-locking is relatively simple; we can try it first. We apply a sinusoidal signal to the PZT-mounted mirror to measure its length, and sense that signal in either the reflected or the transmitted light (with a photodiode on a nearby optical table in air). The servo can be implemented with a signal generator / lock-in amplifier, a filtering amplifier, and a PZT driver. Feedback filters can be easily implemented with an analog amplifier or a suitably-modified PMC servo board. Alternatively, we can implement digital filtering using our digital front end control system, with spare ADC and DAC channels. For initial studies, we plan to use a simple analog servo.

Alternatively, we can acquire a PDH RF signal from the reflected light. There's only one +166 MHz sideband incident on the OMC (due to the detuned SRC), but it should still work. However, will using the RF sideband (+166 MHz) to reflection-lock imprint the very noise we are trying to get away from, onto the transmitted carrier light, thus defeating the primary purpose of homodyne detection?

## 3.4 DC detection photodiodes

A DC photodiode must be isolated from the large amount of low frequency seismic (motional) and acoustic noise in the environment. At the 40m, this is most easily arranged by operating the DC photodiodes on the seismic stacks in the vacuum envelope.

Photodiodes typically are operated with pre-amplifiers mounted together on a PC board; such electronics packages typically are not vacuum compatible. There are several ways to deal with this:

- Use a bare InGaAs photodiode. Electronic signal amplification will occur immediately outside the vacuum chamber feedthrough. We will be susceptible to any magnetic fields or other noise pickup inside the chamber.
- Package the pre-amp inside of a sealed metal case to minimize outgassing in the vacuum.
- Package the entire photodiode and electronics in a partially-pressurized can filled with an inert, RGA detectable gas, and a laser window. Place the whole can in the vacuum chamber.

The first option is the simplest, if the signal maintains its integrity as it exits the chamber. This depends on the potential for noise pickup in the chamber. We believe that this can be minimized, and that this solution is workable. We can fall back on one of the other solutions if necessary.

Ben Abbott has investigated possible materials to make the mounts from, or coat the mounts with, to effectively dissipate heat while remaining vacuum-compatible. He has assembled a prototype mounted photodiode (see Figure 20), and tested its properties under thermal loading. The device was tested in a vacuum bell jar, with 100 mW of thermal loading through a resistor for several days. The temperature rose

by around 4 Kelvin before stabilizing. This puts the operating temperature of the photodiode itself at somewhere slightly above 76 deg. F. This shouldn't pose any threat to the semiconductor material.

We will probably want to install two DC photodiodes at the AS port, one for “in loop” control of DARM and the other as an “out-of-loop” monitor. We will need a beam dump, and maybe a shield for scattered light. A design of a DCPD assembly is in Figure 21.

Intensity fluctuations in the incoming beam from the PSL will couple directly to GW noise at the AS port; therefore, such noise must be sensed and controlled at the same level as the GW signal. We may need to install an ISS photodiode of the same design as the DC photodiode, and on the same in-vacuum optical table. There will be room on the OOC table for all three DC photodiodes. We may want to place the ISS photodiode that senses the MC transmitted light to be on the IOC table, if room can be found.

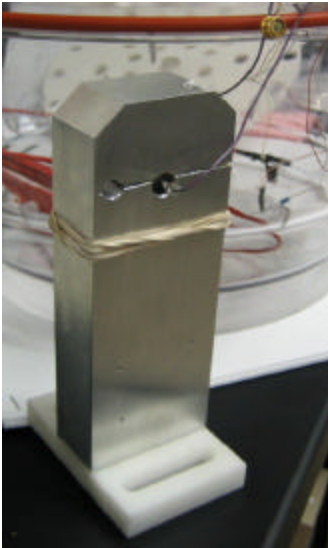


Figure 20: Prototype of an in-vacuum mount for a bare DC photodiode.

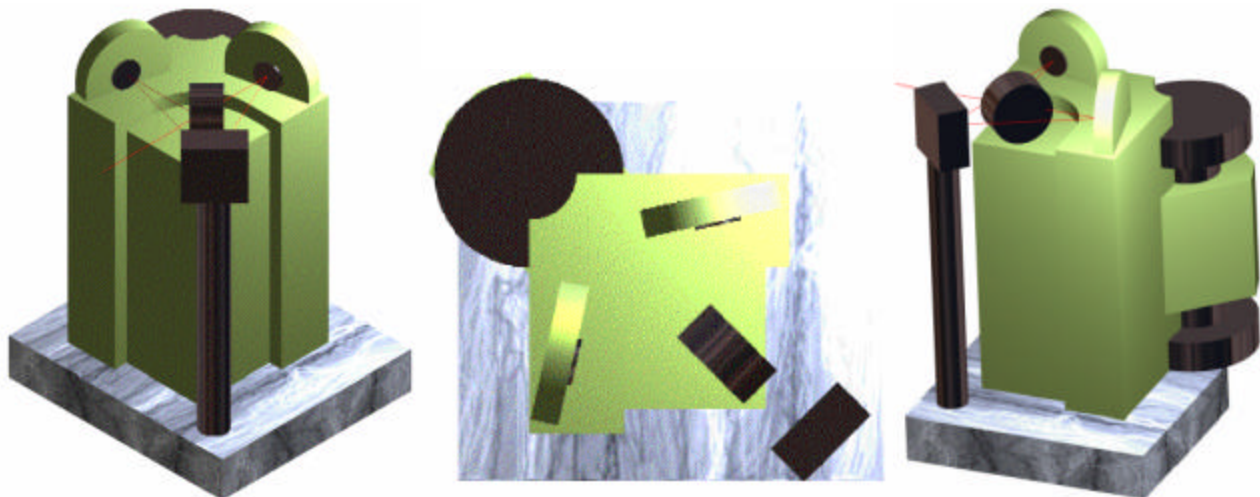


Figure 21: Three views of an in-vacuum DC PD assembly, showing a 50% beamsplitter, two photodiodes, a beam-dump, and a vacuum can to hold electronics. The base will *not* be made of marble.

## 4 Construction and Installation schedule

The primary items to be constructed prior to installation are:

- The in-vacuum PZTs. These can be identical to the ones that are already in use at the 40m for steering the beam from the input mode cleaner to the main IFO.
- The output MMT. This is of very similar design to the system designed, built and installed by Mike Smith for matching the beam from the input mode cleaner to the main IFO.
- The output Mode Cleaner (OMC).
- The DC photodiodes.

It will require roughly two-three months to finalize the design, order, receive, vacuum-prep, assemble and align (in air) all of these devices, given the availability of Mike Smith.

It will take on the order of 1-2 months to vent, install, and coarse-align (in air) all in-vacuum devices. We hope to be able to commission and begin experiments with the DC detection beamline 3-4 months after finalizing the design.

Alignment in the 40m vacuum envelope (in air, during vent) is best done using the main beam from the PSL; however, it is not safe to resonate the beam in the optical cavities, and if there is no resonance, the light exiting the SRM is quite dim. We can, however, bring an autocollimator beam in from a nearby table and align it with the faint beam from the SRM. This will give us plenty of light for coarse alignment of the PZTs, OMMT, OMC, DC PDs, and the exit beams (API, OMCR, OMCT). The steering PZTs (and the focusing picomotor on the OMMT) should give us sufficient control to do fine-alignment after pump-down.

## 5 Budget

This is little more than a ball-park estimate:

Mode matching telescope	3000
6 in-vac fixed steering mirrors	2000
Two PZT steering mirrors	8000
Output mode cleaner	2000
Output mode cleaner controls	5000
DC photodetectors	2000
OMCR beamline	2000
OMCT beamline	2000
Controls and monitoring electronics	4000
<b>TOTAL</b>	<b>30000</b>



## 6 Outstanding questions and further plans

Big questions:

- Given the 40m environment, is the entire task worth pursuing? What will we learn?
- Assuming it is worth pursuing and that we will learn a lot... Is the overall scheme sensible? Are there other / better ways?

Predictions for expected noise sources / couplings:

- laser frequency and intensity noise
  - Just how bad is having the ISS pickoff after the Mach-Zehnder?
  - In-vac sensing?
  - With DC detection, laser intensity noise feeds directly in to the GW signal; it must be suppressed sufficiently well. Need DC photodiode on input light for intensity stabilization to AdLIGO spec.
- Mach-Zehnder phase and amplitude noise
- MICH/PRC/SRC/DARM servo offset/noise couplings
- OMC servo noise, length fluctuations / couplings, RF sideband rejection, HOM rejection
- How much do fluctuations in the loss mismatch 'quadrature' couple into the GW signal?
- Noise couplings can be analyzed using the methods of Camp et al, Mason, Adhikari and Ballmer,...
- Kentaro Somiya accounts for full quantum noise effect, ala Buonanno&Chen.
- Must pursue in parallel with design and construction of engineering prototype of homodyne detection.

Design and implementation considerations:

- OMC: 3-mirror or 4-mirror?
- Locking the OMC: PDH reflection locking? Dither-lock?
- Sensing the OMC-input beam alignment?
- To get the arm-filtered DC light out the AP: offset lock the arms (DARM) or the Michelson (MICH)?

### 6.1 Further Plans

Nergis Mavalvala and Keisuke Goda are preparing a squeezed light source at their lab in MIT, and propose to bring it to the 40m sometime next year, to inject squeezed light into the AS port of the DRFPMI, to measure the effect it has on the noise with homodyne readout.